Bulletin of the Seismological Society of America, Vol. 71, No. 6, pp. 1701-1718, December 1981

A BROADBAND STUDY OF THE 13 AUGUST 1978 SANTA BARBARA EARTHQUAKE

BY TERRY C. WALLACE, DON V. HELMBERGER, AND JOHN E. EBEL*

ABSTRACT

The Santa Barbara earthquake of 13 August 1978, provides an opportunity to perform a broadband investigation of body waves for a well-recorded, moderate size (M_L = 5.1) event. The long- and short-period teleseismic body waves are modeled in the time domain to construct a source time function which is consistent in the period range of 1 to 20 sec. The long-period records indicate an overall duration of 6 sec while the short-period records reveal the fine-scale character of the slip history consisting of two sharp pulses separated by about 1 sec. The source mechanism determined from this analysis is a moderately dipping (30°NE) thrust with significant left-lateral slip. The moment was determined to be 1.1×10^{25} dyne-cm.

The earthquake was also reasonably well recorded on accelerographs in the near-field. The modeling of the strong motion displacements was a two step procedure: (1) the displacements were modeled alone, and (2) in an attempt to achieve consistency between the local and far-field time functions, the qualitative features of the teleseismic short-period time function were used to predict the displacements. If the two sources in the short-period time function are allowed to have different mechanisms, the displacements can be modeled quite well. This suggests that the overall faulting process was rough, and the multiple source character suggested at high frequencies is due to high-stress drop asperities. The two sources are modeled as asperities separated by 1.5 km; the first source has a mechanism consistent with the teleseismic solution while the second source is more steeply dipping. The total moment determined from the strong motion data is 3.5×10^{24} dyne-cm or one-third the long-period moment. This is consistent with other recent studies which suggest that the high-frequency strong ground motion is controlled by the distribution of asperities even though the sum of their moments may be small compared to the overall moment. This study also shows the importance of teleseismic short periods in predicting the local displacements.

INTRODUCTION

The Santa Barbara Channel is one of the more seismically active regions in southern California (Allen *et al.*, 1965) and has been extensively instrumented with accelerographs. Because of the dense instrumentation, the Santa Barbara earthquake of 13 August 1978 was reasonably well recorded in the local field (11 accelerograph sites were triggered) even though it was small (M_L = 5.1, Whitcomb and Hutton, 1978). The event occurred just south of the community of Santa Barbara and caused extensive damage in several neighboring coastal communities. Figure 1 locates the epicenter of the event, the extent of the first day's aftershocks (which is interpreted to be the fault plane), and four strong motion sites which are modeled in this study.

The horizontal accelerations at the two nearest stations, UCSB and SBCH, were rotated into radial and tangential components as shown in Figure 2. These records

* Present address: Weston Observatory, Boston College, Weston, Massachusetts 02193.

are interesting for several reasons; first the peak accelerations are surprisingly high considering the earthquake's magnitude and second, although the records are complicated they appear to display coherence. The coherence is remarkable considering the difference in distance and azimuth between the stations and the strong

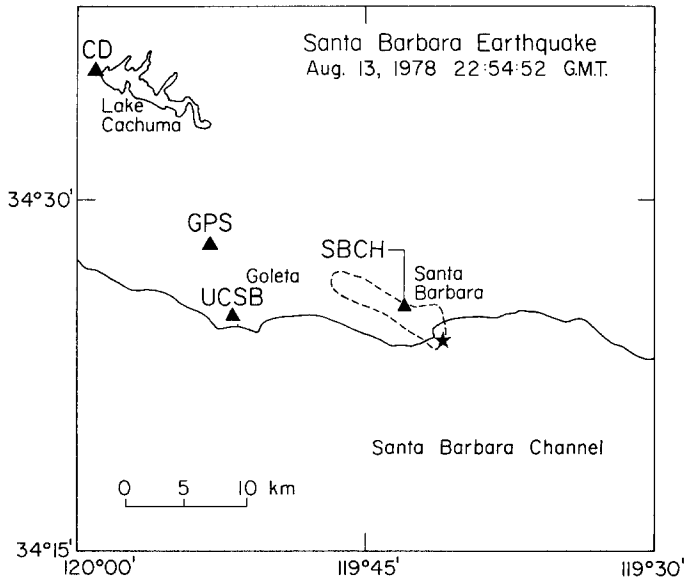

FIG. 1. The location of the Santa Barbara earthquake, the aftershock zone (dashed line), and four accelerograph sites which are modeled in this study.

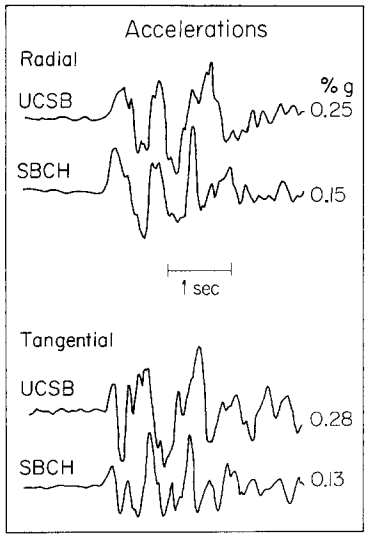

FIG. 2. The horizontal accelerations from the two closest recording sites. Both components appear quite coherent; this suggests the main waveform structure is due to the time function which can be represented as a series of sources.

structural heterogeneity typical of this region. These records suggest that, even though this event was small, the faulting process was rough; high-stress drop asperities probably were important.

The Santa Barbara earthquake also produced short- and long-period observations

on a global scale providing an opportunity to perform a broadband investigation of the body waves. The local accelerographs and teleseismic WWSSN records allow the determination of the source parameters in the period range of 1 to 20 sec. Recently, several authors (Hartzell, 1980; Ebel and Helmberger, 1981) have studied the faulting process over a similar frequency range for somewhat larger events. As expected, they found that the shorter period records contain more detailed information about the faulting process. The advantage of studying the Santa Barbara earthquake is that its moderate size should be reflected in a simple source model, and any effects of directivity, multiple sources (asperities), and crustal structure can be readily isolated. The broadband investigation of body waves allows the relationship between the local strong motions and teleseismic signals to be more fully explored. In particular, we want to be able to design a source time function which will adequately model the body waves over the entire frequency range. This should answer questions about the ability to see asperities in both the local and teleseismic data, and whether the different records can be used to predict each other. We will consider these possibilities in this report.

Tectonic Setting

The Santa Barbara earthquake occurred in the Santa Barbara Channel which is a trough that defines the western extent of the Transverse Ranges province. Throughout the Transverse Ranges province, north-south shortening appears to be taking place (Pechmann, 1979; Savage *et al.*, 1978). This shortening is reflected in the channel by the rate of coastal uplift which has averaged up to 10 m/1000 yr over the last 45,000 yr (Lee *et al.*, 1978). This environment is likely to give rise to extreme structural heterogeneity. The Santa Barbara Channel has experienced at least three noteworthy historical events. They are: (1) a large 1812 event which generated a sizable tsunami; (2) a magnitude 6.3 event in 1925; and (3) a magnitude 5.9 event in 1941 (Sylvester *et al.*, 1970). Earthquakes throughout the Transverse Ranges typically have thrusting mechanisms with some left-lateral component.

The 13 August 1978 event caused in excess of 7 million dollars of damage (Miller and Felszeghy, 1978), although no onshore surface faulting has been detected. There is an apparent asymmetry in the intensity of shaking, with regions northwest of the epicenter subject to more intense shaking. Some areas in Goleta experienced peak accelerations of 0.44 g (North Hall on the UCSB Campus) while downtown Santa Barbara, which is half the distance to epicenter, only experienced 0.21 g. In the aftershock zone outlined in Figure 1, the very first aftershocks were in the northwest end (Corbett and Johnson, 1981). As time progressed, the aftershocks then occurred throughout the zone. The asymmetric intensity of shaking and mode of aftershock occurrence suggests that directivity may be important with the rupture propagating from the southeast end of the fault toward the northwest.

Teleseismic and Regional Body-Wave Analysis

The analysis of the far-field data was conducted in three parts in an attempt to isolate any dependence of the fault parameters on the period range of the data set. First, the long-period data was analyzed alone, then the short periods, and finally the short and long periods were simultaneously analyzed. The analysis includes determination of the focal mechanism, source time function, moment, and stress drop. The waveforms of about 50 WWSSN and Canadian network stations were recovered for the event. Unfortunately, because of the type, size, and location of the

event, it was not well recorded in the Pacific (the southwest quadrant of the focal sphere). All the first motions are compressional and thus, indeterminate for constraining the fault planes (see Figure 3). Although the fault plane was not well constrained by the first motions, it is possible to find a fault orientation which satisfactorily explains the waveforms by fitting synthetic seismograms to the observations.

Long-period body waves. The analysis of the long-period body waves consists of matching the observed teleseismic waveforms with synthetic seismograms computed with generalized rays for a point shear dislocation (see Helmberger, 1974; Langston and Helmberger, 1975). For teleseismic P waves, three basic rays are used: P; pP; and sP. Additional rays may be introduced by near-source or near-receiver crustal

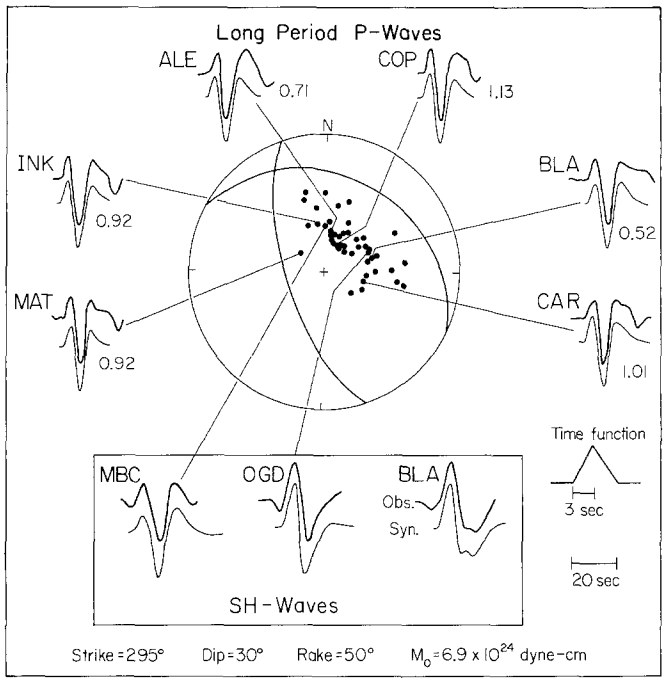

FIG. 3. Summary of the long-period body-wave analysis. Fifteen P waves were modeled to determine the mechanism and moment. Shown are six representative P waves and their synthetic fits. Also shown on each trace is the ratio of the station moment to the average moment. Three naturally rotated SH waves and their synthetic fits are also shown.

structure. An example of this would be S-to-P and P-to-S conversions at the Moho. The synthetic seismogram is the sum of the displacements associated with these rays multiplied by an appropriate receiver function and convolved with an instrument, an attenuation operator, travel path structure, and a source time function. P waves recorded at distances between 30° and 90° have travel paths in the lower mantle and the waveforms are free of the effects of the upper mantle triplications, so the travel-path operator is presumed to be a delta function. Studies of other earthquakes in this region (Burdick and Mellman, 1976; Ebel *et al.*, 1978) have used high values of t^* in their attenuation operators, so as a starting model, values of t^* = 1.0 sec for P waves and 4.0 sec for S waves were used. Several complicated crustal models have been used for studies of local short-period data (Lee *et al.*, 1978; Corbett and Johnson, 1981), but it was found that these models did not greatly

change the synthetic waveforms so an average model was used. This crustal model is shown in Table 1. The modeling procedure was essentially a trial-and-error fit of the synthetics to the observations. The best fit was obtained in terms of the following parameters: source depth; source orientation; and a time function. The source time function was parameterized in the form of a trapezoid as described by Helmberger and Malone (1975). Note that the second pulse in the observed records (Figure 3) usually has a larger area than the synthetics. This is probably due to *S*-to-*P* and *P*-to-*S* conversions in near-source and receiver structure, but the inconsistency is not systematic or large enough to warrant a more complicated crustal model, so the simple structure was assumed in the trial-and-error process.

The long-period *P* waves from 15 records beyond 30° were modeled. Figure 3 summarizes the analysis; shown are several representative *P* waves and their synthetic fits. Note that the waveforms at all the stations are similar and simple; a single point source is sufficient to model the *P* waves. The major parameter controlling the fit of the synthetics to the data is the pulse width, which is a function of the source time function and the depth of the event. Using the average crustal model, the best-fitting depth is 12 km. This source depth compares favorably with the 12.8-km depth determined by Corbett and Johnson (1981) using the standard

TABLE 1

CRUSTAL MODEL

V_p (km/sec)	V_s (km/sec)	Density (gm/cm^3)
5.5	3.1	2.5

Caltech hypocenter program. This agreement suggests that our average velocity model is a good approximation of the true velocity structure, and that the inaccuracies in our velocity model do not affect the general conclusions of this study. The time function is a symmetric triangle with a 6-sec duration. The time function is not unique and a trapezoid with a shorter duration can be used ($t_1 = 2$ sec, $t_2 = 1$ sec, $t_3 = 2$ sec). The focal mechanism has a strike of 295°, a dip of 30°, and a rake of 50°.

Also shown are some *SH* waves which were useful in constraining the solution. Unfortunately, the size and type of event was such that the *S* waves were not well recorded beyond 50°. Because of the strong *SV*-coupled *PL* in the distance range of 35° to 50°, only those stations which were naturally rotated were used in the *SH* modeling. From this analysis it is apparent that although the fault plane is not well constrained, the long-period body waves are explained by a simple model. The *S* waves on the East Coast of the United States provide the best constraint on dip, and the *P* wave at station MAT is particularly sensitive to rake. The strike of the northeast-dipping plane is consistent with the trend of the aftershocks (see Figure 1).

The Santa Barbara earthquake was cleanly recorded at only two stations at distances less than 12°: ALQ and COR. Wallace *et al.* (1981) developed a technique for the inversion of *Pn* and *PL* recorded on long-period vertical and radial instruments to determine the focal mechanism. This technique was applied to the waveforms at ALQ and COR, and Figure 4 shows the data and synthetics for the inversion solution. The best-fitting model for the regional data is consistent with the teleseismic modeling. Several authors have determined a focal mechanism for this event on the basis of local short-period data. Their solutions are summarized in Table 2. These solutions are similar to ours, although the mechanisms determined with local data are very sensitive to the crustal model assumed.

The seismic moment of this event was calculated by comparing the observed amplitudes with the synthetics. Assuming a $t^* = 1.0$ sec, the moment determined from 15 *P*-wave observations is 6.9×10^{24} dyne-cm. Shown next to each synthetic trace in Figure 3 is the ratio of the station's moment and the average moment. This ratio serves as a measure of amplitude stability. The amplitude agreement in this study is as good or better than other comparable studies. In addition to the focal mechanism and moment, several other source characteristics such as stress drop and average displacement can be obtained from the body-wave analysis by making some estimate of the fault dimensions. The fault area was estimated from the areal extent of the first day's aftershocks. The length of the fault appears to be about 10

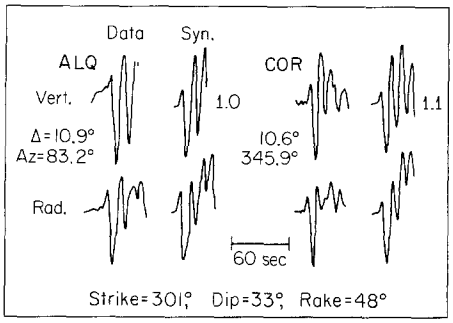

FIG. 4. Regional *Pn* and *PL* data. The numbers to the *left* of the vertical traces give the moment ($\times 10^{25}$ dyne-cm) for the mechanism shown.

TABLE 2

LOCAL FAULT PLANE SOLUTIONS

Strike (°)	Dip (°)	Rake (°)	Reference
294	40	57	Lee *et al.* (1978)
280	26	57	Corbett and Johnson (1981)
295	30	50	This study

km, with about a 5-km width. Assuming a rectangular fault, we can relate stress drop to fault dimensions and moment (Aki, 1966; Kanamori and Anderson, 1975) by equation (1)

$$\Delta\sigma \simeq M_0/W^2L \tag{1}$$

where W and L are the width and length of the fault, respectively. Using this relationship, a stress drop of 28 bars is obtained with an average displacement of 46 cm.

Short-period body waves. The short-period data set consists of only six records in which the signal-to-noise ratio was sufficiently large, but fortunately the azimuthal coverage is fairly good. Figure 5 shows the waveforms; note that records along similar azimuths appear to be coherent for 8 to 10 sec. This azimuthal coherence suggests that for these waveforms the receiver structure is not of primary importance and source information can be readily extracted. Stations to the northeast (COL and INK) are essentially three pulses and appear longer period than those stations to the east (BLA and SJG). Also consider the stations in order along strike from the northwest to the southeast. The waveform is simple at COL and INK, at MBC an additional spike appears in the first downswing. This additional spike is well

developed at FRB; the waveform is characterized by three higher frequency pulses and a somewhat delayed fourth pulse. This waveform persists at BLA and SJG. This suggests that some type of directivity effect is present, possibly multiple sources rupturing from southeast to northwest.

The short-period modeling procedure is analogous to that for the long periods, in that synthetics are computed for point sources and convolved with an appropriate attenuation filter, a WWSSN short-period instrument response, and a source time function. The same crustal structure and t^* as used in the long-period analysis was

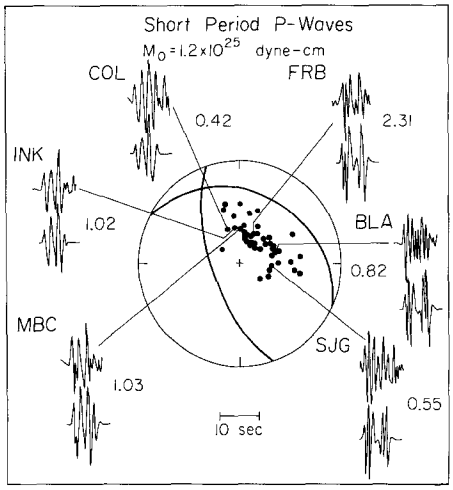

FIG. 5. Summary of the teleseismic short-period analysis. The ratio of the station moment to the average moment is given for each station.

TABLE 3

SHORT-PERIOD SOURCE PARAMETERS

Source	Strike (°)	Dip (°)	Rake (°)	X^*	Y^*	Depth (km)	Time Lag (sec)
1	298	34	43	0	0	8.6	0
2	299	33	47	2.3	1.1	8.2	0.6

* X refers to the distance along strike in kilometers and Y refers to distance perpendicular to strike.

used here. From the discussion above it appears that the short-period time function requires multiple sources. Since this significantly expands the model space to be investigated, a least-squares waveform inversion technique was employed. The technique involves an iterative scheme which makes use of an error function determined by the cross-correlation of the observed waveform and synthetic (Burdick and Mellman, 1976; Mellman 1978; Ebel and Helmberger 1981). The error function is minimized in terms of the number of sources, source depth, source orientation, and time function.

The final inversion model is shown in Figure 5. The records can be adequately modeled with two sources which have triangular time functions. Table 3 summarizes the inversion model. Note that the second source is down strike from the first suggesting a rupture mode consistent with the aftershocks. The two sources have similar orientations, which are consistent with the long-period faulting mechanism. Both sources have a depth of approximately 9 km. Since the short periods have a less severe trade-off between source depth and time function duration, it is likely that for the average crustal model the short-period depth is better. If these sources

are interpreted as asperities, then they appear to reflect the regional stress regime, unlike some other earthquake studies with multiple sources (Burdick and Mellman, 1976). The spatial and temporal differences between the sources suggests an abnormally high-rupture velocity. This is an artifact of the inversion and because spatial resolution is poor the 2.6 km separation is hardly unique. In Figure 5, the ratios of station moment to the average moment is shown; note that the moment determined from the short periods is larger than that determined for the long periods. This

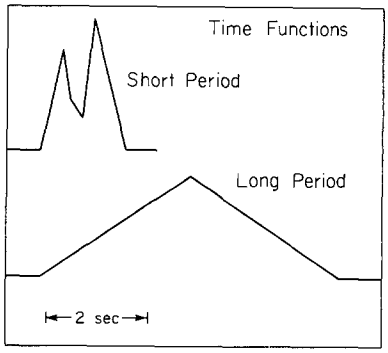

FIG. 6. Comparison of the short- and long-period time functions.

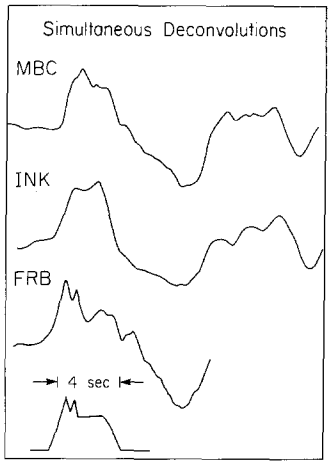

FIG. 7. Simultaneous deconvolution of the short- and long-period data at three stations. The first 4 sec mark the arrival of the P wave and indicate the form of the time function.

suggests that either the long-period time function is incorrect or that the value of t^* is inappropriate.

Simultaneous short-/long-period analysis. Figure 6 shows a comparison of the time function determined for the long periods and that determined for the short periods. As expected, the short periods contain much more detailed information about the faulting process. These time functions must be combined to give a source time function which will fit both period ranges. The first step in this process is to check the compatibility of the short- and long-period waveforms. This is done by a simultaneous deconvolution procedure outlined in Burdick (1977). For each station, the short- and long-period records are passed through a Gaussian filter and the

instrument and attenuation operators are divided out of the response. The spectra of the two deconvolved ground motion responses are added together; the information in the frequency range where the two instruments overlap (0.125 to 0.5 Hz) is averaged. The summed response is transformed back into the time domain to obtain the broadband ground motion. The ground motion is reconvolved with the instruments and attenuation operator and compared to the original seismograms to assure stability of the procedure.

The simultaneous deconvolutions for the three stations with the best long- and short-period seismograms are shown in Figure 7. A $t^* = 1.0$ sec and a half-width of

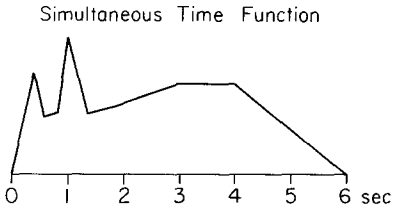

FIG. 8. Time function derived from simultaneous analysis of the short- and long-period data.

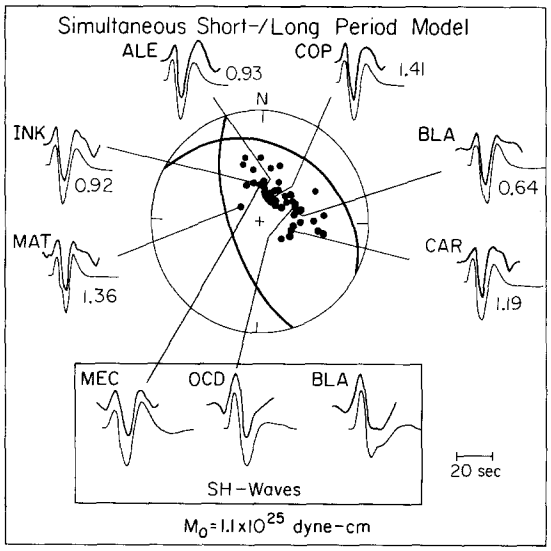

FIG. 9. Recomputation of long-period synthetics for simultaneous time function. Moment ratios are shown for representative stations.

0.75 sec were used in the Futterman attenuation operator and the Gaussian filter, respectively. What we have attempted to do in the deconvolution process is to isolate the time function; the first upswing of the deconvolution corresponds to the arrival of the P wave and should be representative of the time function. At all three stations, the basic time function appears to be a 4-sec trapezoid. Superimposed on the trapezoid is some higher frequency structure which can best be seen at FRB. Shown below FRB in Figure 7 is the time function inferred from the deconvolution process. It appears to preserve the essence of the previous analysis in that there are two short-period sources superimposed on a long-period source.

The success of the deconvolutions suggests that a single time function could satisfactorily explain both the long- and short-periods. To obtain the time function, all the records were used in the inversion routine. The short-period time function

was fixed to be the one shown in Figure 6, and the long-period source was allowed to vary. In an effort to correct for the short-period moment being larger than the long-period moment, t^* was adjusted until the moments were in agreement. This yielded a $t^* = 0.7$ sec for P waves. This gives a long-period moment which is

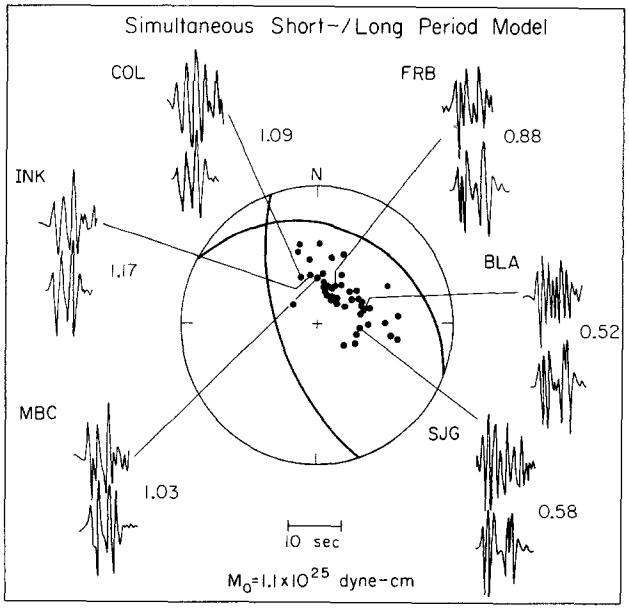

FIG. 10. Short-period synthetics for the simultaneous time function.

TABLE 4

SOURCE PARAMETERS FOR THE SANTA BARBARA EARTHQUAKE

Date:	13 August 1978
Origin time:	22h 54m 52.4s UTC (Caltech)
Location:	34°23.92'N 119°40.88'W (Corbett and Johnson, 1981)
Depth:	12 km
Magnitude:	$M_L = 5.1$
	$m_b = 5.5$
	$M_S = 5.6$
Mechanism:	Strike = 295°
	Dip = 30°N
	Rake = 50°
Moment:	1.1×10^{25} dyne-cm
Fault area:	50 km^2
Stress drop:	44 bars
Average dislocation:	73 cm

consistent with that determined from the regional seismograms in Figure 4 where no attenuation operator is used. Using the adjusted value of t^*, the simultaneous time function shown in Figure 8 was determined. This time function is considerably more complex than would be inferred from the teleseismic long periods alone. Figures 9 and 10 show the synthetic fits to the data with this new time function. Table 4 summarizes the teleseismic source parameters for the Santa Barbara earthquake. Stress drop and average displacement are calculated from (1).

Strong Ground-Motion Analysis

The strong motion analysis consists of modeling the displacement records at four sites. In addition, the tangential velocity records at the three sites closest to the epicenter were analyzed in detail to investigate the location and strength of asperities. The procedure is the same as before; a model is derived on the basis of the displacements alone and then we attempt to make it consistent with the teleseismic model.

The four stations which we used in this analysis where chosen on the basis of their location and the size of the displacement signal. It was assumed that the corrected accelerograms, and hence the displacement signals were not influenced by the structure which housed the instruments. The horizontal components of displacement at each station were rotated into the radial and tangential displacements. Figure 11 shows the rotated displacements for all the stations. The modeling

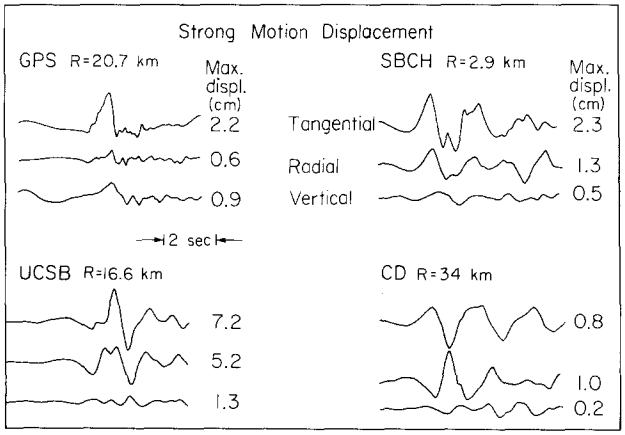

FIG. 11. Strong motion displacement records for the four sites modeled in this study. The records have been rotated into the tangential and radial components.

procedure consists of comparing the synthetic to the horizontal displacements, emphasizing the fit of the tangential waveforms. The relative amplitude of the vertical displacement was used as a constraint in the modeling, but in general, the vertical waveforms were not heavily weighted. There are several reasons for this: (1) for the small ranges which are dealt with in this study, structure most affects the vertical and radial components; (2) in general, the amplitude of the vertical components were small compared to the horizontal displacements; and (3) there is a periodic ringing in the vertical accelerograms, especially at UCSB and SBCH. Assuming that the epicenter is located in the channel, this ringing could represent multiple bounces in the shallow coastal structure.

The synthetics were calculated using the generalized ray methods for point shear dislocations. The response at a particular point is represented by the sum of the individual rays which traverse different travel paths. It is assumed that the faulting process can be represented by a series of point sources. The response of each generalized ray was calculated using the Cagniard-de Hoop technique. For all the stations except SBCH, it was sufficient and justifiable to use the asymptotic solution (see Helmberger and Harkrider, 1978). For SBCH, which is very close to the epicenter, it is apparent that near-field effects are important and the exact solution

has to be used. Both the asymptotic and exact solutions have been employed to successfully model strong ground motion in previous studies (Heaton and Helmberger, 1978, 1979). Once the synthetic displacements are computed they are Ormsby-filtered so they can be compared to the observations.

A significant feature of the horizontal displacements in Figure 11 is their simple, single-pulse nature. The intense shaking was confined to 1 or 2 sec and the tangential displacement records are dominated by a triangular pulse. This is most obvious at GPS, where the tangential triangular pulse is the only significant displacement. This suggests that in the period range of 2 to 3 sec, the source is fairly simple. On the basis of displacements alone, a single point source located at the hypocenter is sufficient for the modeling procedure. Note the UCSB and GPS are essentially along

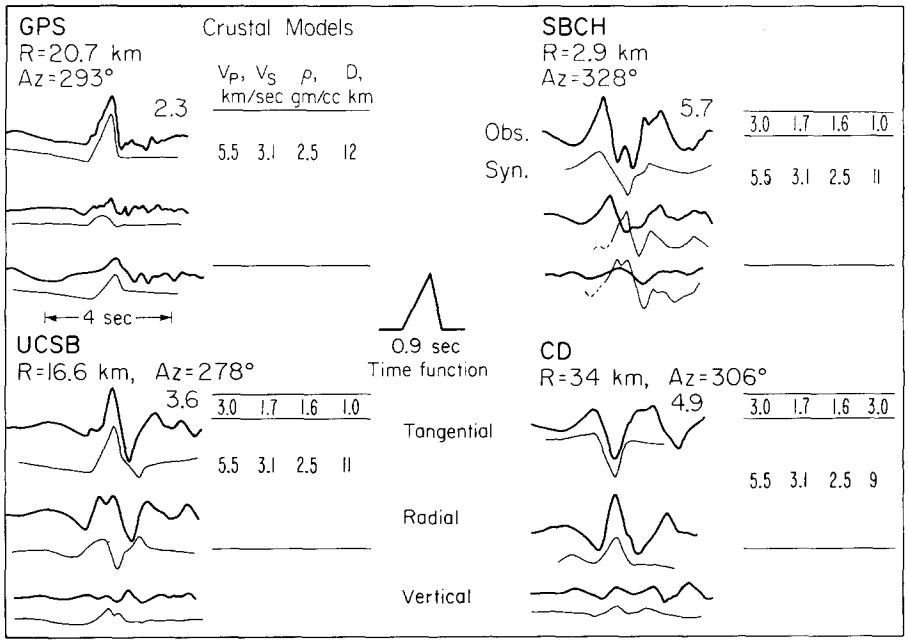

FIG. 12. Fit of the synthetics for a single point source to the displacements. The crustal structure used at each site is shown to the *right*. Above each tangential trace is the moment ($\times 10^{24}$ dyne-cm) determined at that station.

strike of the aftershock zone (see Figure 1), and although the stations are of similar azimuth and range, the waveforms are not very coherent; in particular, note the importance of the relative amplitudes of the radial and tangential components. The absolute amplitudes are also significantly different. GPS is only 4 km further from the epicenter than UCSB, yet the amplitude of the tangential displacement is one-third as large. This is surprising considering the apparent coherence of the accelerations. This suggests strong structural heterogeneity. In an attempt to account for this, the receiver structure was varied at each station. The complex geology of the region justifies this since rapid changes in structure would be expected.

The GPS record is so simple that it is assumed that the tangential pulse is just a direct *SH* arrival. The source time function essentially could be measured off the displacement trace. The time function is sufficient for the other stations; Figure 12 shows the synthetic fits to the displacements for the best-fitting model. The shallow receiver structure used for each station are shown to the *right* in Figure 12. Absolute travel time, in other words the *S-P* time (assuming the instrument triggered on the

P arrival), was only approximately fit. The data and synthetics were aligned such that the tangential waveform was best fit. Also shown in Figure 12 is the moment ($\times 10^{24}$ dyne-cm) computed for the tangential component at each station. All three components at GPS are fit very well with a simple half-space. UCSB requires slow sediments to increase the amplitude of the radial component although the synthetic amplitude is still too small. The tangential pulse at UCSB is shorter period and more complex than at GPS.

The SBCH records show what appears to be a noncausal drift on both the displacement and velocity records characteristic of a station in the near-field, and in addition, the assumption of a point source probably is poorly justified considering the source-to-receiver distance. The near-field component of displacement results in some static offset which is manifested as a noncausal drift when Ormsby-filtered. (The small range of SBCH implies that a slight mislocation of the epicenter can result in large changes in azimuth and hence the mechanism that would be inferred from displacements is also subject to large uncertainty.) In fact, the azimuth was set at 340° for the synthetics in Figure 12. Considering the importance of the Ormsby filter to appearance of the synthetics, the fit is fairly satisfactory at SBCH. CD is the furthest station from the epicenter, but had the largest arrival time-trigger time of 3 sec. This suggests that the CD instrument did not trigger on the *P* arrival, triggering instead on some other arrival, possibly the *S* arrival. Because of this, we fit the waveforms as if they were a multiple from a lower velocity layer over the half-space. For this reason, no confidence is assigned to the CD waveform fit; the useful information obtained from the modeling is a constraint on the strong motion moment.

The fault plane solution inferred from the strong motion displacements is significantly different from that determined from the teleseismic data; the strike = 295°, dip = 60°NE, and rake = 60°. Although the strike and rake are consistent between the two solutions, the steepness of dip is not. GPS, which is essentially on strike, provides a good constraint on dip. If the fault plane is dipping as shallow is 30°, the tangential pulse would be nodal or negative. There is no plane-layered structure which will reverse the polarity of the strong, simple tangential component at GPS. This suggests either the strong motion is associated with a steeply dipping fault or that we have to resort to severe crustal structure such as layers with near-vertical attitudes to reconcile the near- and far-field observations. Another constraint on the dip is the uniform lack of strong vertical components of displacement. A thrust event on a shallow-dipping plane, even with a large strike-slip component, will produce significant vertical accelerations at SBCH, GPS, and UCSB. These observations indicate that it is not possible to model the strong ground motion displacements with the long-period faulting mechanism and a single point source in a plane-layered crust.

A weighted average of the seismic moments determined from each of the tangential components of displacement yields a strong motion moment of 3.5×10^{24} dyne-cm. This average moment is roughly one-third that determined from the teleseismic analysis. This is consistent with the fact that asperities (zones of high-stress drop) would efficiently radiate high-frequency seismic energy while the other part of the fault plane may not. Note that the station moments computed for a single point source do not vary in a systematic way that would suggest directivity effects consistent with a southeast to northwest rupture.

This strong motion time function is not compatible with the teleseismic time function. The short-period time function should be reflected in the near-field;

although there is a hint of two sources at UCSB and SBCH, one source is fairly successful in explaining the records. A closer look at the short-period time function shows that the second source is downstrike of the first source. Since GPS and UCSB are on strike, if a reasonable rupture velocity is assumed it is quite possible that the two sources constructively interfere. SBCH, which is offstrike and very close to the epicenter, should show the two sources best; note that the SBCH records do in fact most strongly suggest two sources.

The obvious test for multiple sources is to use the teleseismic short-period time function for the strong motion synthetics. Figure 13 shows a comparison between the data and the synthetics for this case. The distance between the two sources has been adjusted to be 1.5 km to better fit the SBCH record. Note that the amplitudes of the synthetics are much too large. This is because the teleseismic short-period moment is so large; the moment could be significantly overestimated since it is an

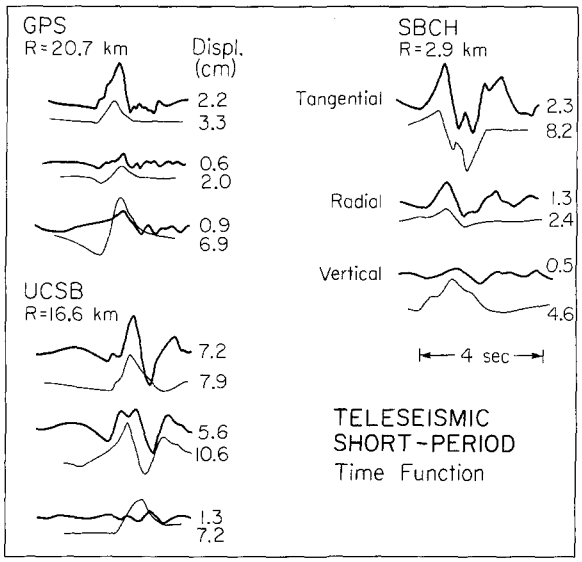

FIG. 13. Fit of the synthetics using the teleseismic short-period time function. On each trace is the displacement in centimeters.

average of only six observations (note the very large value at FRB) or if an error in t^* exists. The strong motion tangential records fit fairly well with this time function. The vertical displacements are systematically too large, the effects of which have been discussed previously.

Using the short-period teleseismic time function as a starting model, the strong motion time function can be fine-tuned to improve the fit of the displacements. With the paucity of data it is very difficult to investigate interfering sources in the frequency range of the displacement records. In order to obtain better resolution the tangential velocity traces were used. Figure 14 shows the velocity traces, the synthetics for the one-source model derived from the displacements and the synthetics for the best two-source model. Because of the nonuniqueness involved, a couple of restrictions were imposed in deriving the two-source model: (1) the first source had to have a faulting mechanism which is consistent with the teleseismic mechanism, and (2) the second source has a strike consistent with the aftershock zone.

The two-source model has the second source larger than the first, so the waveforms at GPS and UCSB are dominated by it. The mechanism of the second source is consistent with that determined for the displacement mechanism. Figure 15 shows a cartoon of the fault model. The sources are separated by 1.5 km and 0.65 sec in time (corresponding to a rupture velocity of 2.3 km/sec) and have a combined moment of 3.6×10^{24} dyne-cm. Considering the nonuniqueness involved in both the

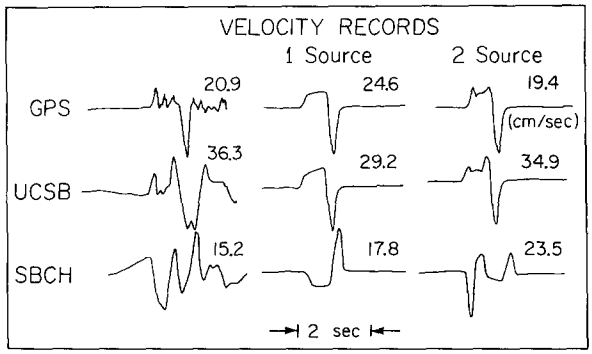

FIG. 14. Tangential velocity records for the three closest stations. Also shown are the synthetics of the one- and two-source models computed in a half-space.

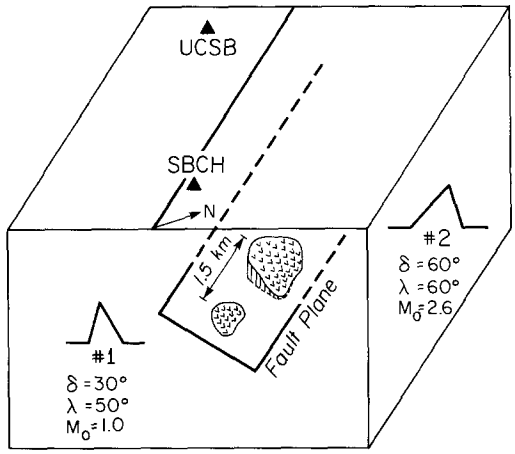

FIG. 15. Schematic of the portion of the fault plane which contains the asperities controlling the high-frequency radiation. The first source has a rise time of 0.2 sec and fall time of 0.4 sec. The second source has a rise time of 0.6 sec and a fall of 0.2 sec. The moments are $\times 10^{24}$ dyne-cm.

determination of the teleseismic short-period source and the strong motion source, the two time functions are consistent. The local field data require the second source to be much more steeply dipping and larger than the first source. This can also be made consistent with the short-period teleseimic data when considering the location of the recording stations on a focal sphere; there is a trade-off between dip and moment. The moment of the second source is only one-fourth that of the total long-period moment so the steep dip of the asperity could well be hidden in the long-period time function.

Figure 16 shows the fit of the two-source model synthetics (computed with the structures shown in Figure 10) to the strong motion displacements. The fits are as good or better than the fits for the one-source model; in particular, the SBCH records. Shown above the tangential component at each station is the ratio of the

observed amplitude to the predicted amplitude. The tangential amplitude agreement is much better than for the one-source model.

Discussion

The investigation of the body waves from the Santa Barbara earthquake in several frequency bands allows us to construct a source time function which is consistent with both near-field and far-field observations. It is also important to note that for even moderate-size events, the band-limited time functions can be significantly different between the short and long periods. This suggests that extreme care should be taken when comparing body waves from different frequency ranges for such procedures as determining t^* from spectra.

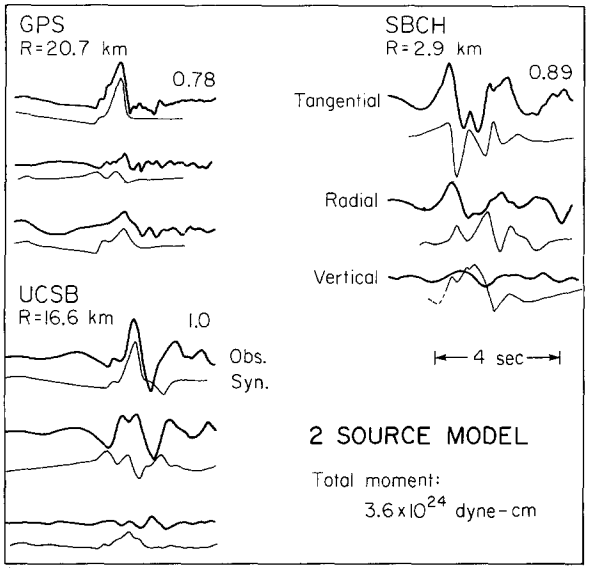

FIG. 16. Fit of the displacements for the two-source model with the crustal models shown in Figure 12. The numbers above the tangential traces give the ratio of predicted amplitude to observed.

Numerous authors (Hart *et al.*, 1977; Lay and Kanamori, 1980; Ebel, 1980; Boatwright, 1980; to name a few) have noted a large discrepancy between the moments computed with body and surface waves. Lay and Kanamori (1980) suggest the reason for this is that, relative to the area which radiates the long-period surface waves, the body waves are radiated from substantially smaller, strongly coupled, isolated regions. The reason for the frequency dependence of the body-wave source time function in this study is similar to the body-/surface-wave moment discrepancy; patches of the fault are more efficient in radiating high-frequency seismic energy than the fault taken as a whole. These patches, or asperities, may contribute only a fraction of the body wave moment, but they are the controlling feature for the radiation of the high-frequency energy; presumably they have a much higher stress drop than the rest of the fault plane. It has been proposed by many authors (Wyss and Brune, 1967; Kanamori and Stewart, 1978; Hartzell, 1980; to name a few) that large earthquakes are a combination of multiple sources. The fact that the multiple source concept can be scaled down to the size of the Santa Barbara earthquake is important in predicting the strong ground motion for moderate-size events.

The time function determined from the teleseismic short periods can be very useful in predicting the time function appropriate for the strong motion. On the

other hand, for events as small as the Santa Barbara earthquake, the teleseismic long periods usually do not contain sufficient high-frequency information to be useful in predicting the strong ground motion. The suggestion that the strong ground motion is controlled by the distribution of asperities has been advanced recently by other authors (Ebel and Helmberger, 1981). This seems to be the case for Santa Barbara, and since it is unlikely that a fault plane 10 km long would be smooth, the fact that the asperity which was primarily the source of acceleration should have a steeper orientation than the overall fault plane is not surprising. The process of smooth rupture and directivity apparently had little effect on the observed ground motion. Directivity is important in the sense that the fault ruptured from southeast to northwest and the timing of the asperity failures were controlled by the rupture velocity. But the scaling factor which controls the size of the accelerations was not the distance from the inferred fault plane, rather the distance from the largest asperity.

The small M_L obtained by Whitcomb and Hutton (1978) for this event seems inconsistent with both the accelerations observed and the moment calculated from the teleseismic body waves. One explanation for this discrepancy may be that all the Caltech Wood-Anderson instruments are in a narrow range of azimuths and are sampling an insufficient range of the radiation pattern. The M_L determined from northern California data is significantly larger; $M_L = 5.7$. Jennings (1979) determined a $M_L = 5.8$ from seismoscopes in the local field. These two higher values for magnitude are much more consistent with the computed moment.

Conclusions

The Santa Barbara earthquake of 13 August 1978 was a moderate-size thrust event with a significant left-lateral strike-slip component. The seismic moment from the simultaneous analysis of the teleseismic long and short periods is 1.1×10^{25} dyne-cm. At long periods (20 sec), the body waves are simple and represent seismic radiation from the entire 10-km fault length. At shorter periods (0.5 to 2 sec), the body waves are more complex due to the presence of two asperities. The strong ground motion is apparently controlled by the high-stress drop asperities even though the sum of their moments is small compared to the moment computed for the overall fault. Since the teleseismic short-period waveforms reflect the roughness of faulting they can be very useful in a qualitative fashion for predicting the strong ground motion of moderate-size earthquakes.

Acknowledgments

The authors wish to thank Thorne Lay and Tom Heaton for many useful discussions. Thorne Lay also read the manuscript and made useful suggestions. Dave Boore reviewed the manuscript and made comments which helped improve the quality of it. Research was supported by the Earth Sciences Section, National Science Foundation Grant PER-7921769.

References

Aki, K. (1960). Generation and propagation of G waves from the Niigata earthquake of June 16, 1964, *Bull. Earthquake Res. Inst., Tokyo Univ.* **44,** 23–88.

Allen, C. R., P. St. Amand, C. F. Richter, and J. M. Nordquist (1965). Relationship between seismicity and geologic structure in the southern California region, *Bull. Seism. Soc. Am.* **55,** 753–797.

Boatwright, J.. (1980). Preliminary body-wave analysis of the St. Elias, Alaska, earthquake of February 28, 1979, *Bull. Seism. Soc. Am.* **70,** 419–436.

Burdick, L. J. (1977). Broad-band seismic studies of bodywaves. *Ph.D. Thesis,* California Institute of Technology, Pasadena, 151 pp.

Burdick, L. J. and G. R. Mellman (1976). Inversion of the body waves from the Borrego Mountain earthquake to the source mechanism, *Bull. Seism. Soc. Am.* **66,** 1485–1499.

Corbett, E. J. and C. E. Johnson (1981). The Santa Barbara, California earthquake of August 13, 1978 (submitted for publication).

Ebel, J. E. (1980). Source processes of the 1965 New Hebrides Island earthquakes inferred from teleseismic waveforms, *Geophys. J.* **63,** 381–403.

Ebel, J. E. and D. V. Helmberger (1981). *P*-wave complexity and fault asperities: the Borrego Mountain, California, earthquake of 1968 (submitted for publication).

Ebel, J. E., L. J. Burdick, and G. S. Stewart (1978). The source mechanism of the August 7, 1966 El Golfo earthquake, *Bull. Seism. Soc., Am.* **68,** 1281–1292.

Hart, R. S., R. Butler, and H. Kanamori (1977). Surface wave constraints on the August 1, 1975 Oroville earthquake, *Bull. Seism. Soc. Am.* **67,** 1–8.

Hartzell, S. (1980). Faulting process of the May 17, 1976 Gazli, U.S.S.R. earthquake, *Bull. Seism. Soc. Am.* **70,** 1715–1736.

Heaton, T. H. and D. V. Helmberger (1978). Predictability of strong ground motion in the Imperial Valley: modeling the *M* 4.9, November 4, 1976, Brawley earthquake, *Bull. Seism. Soc. Am.* **68,** 31–48.

Heaton, T. H. and D. V. Helmberger (1979). Generalized ray models of the San Fernando earthquake, *Bull. Seism. Soc. Am.* **69,** 1311–1341.

Helmberger, D. V. (1974). Generalized ray theory for shear dislocations, *Bull. Seism. Soc. Am.* **62,** 61–589.

Helmberger, D. V. and D. G. Harkrider (1978). Modeling earthquakes with generalized ray theory, in *Modern Problems in Elastic Wave Propagation*, J. Miklowitz and J. Achenbach, Editors, John Wiley and Sons, New York.

Helmberger, D. V. and S. D. Malone (1975). Modeling local earthquakes as shear dislocations in a layered halfspace, *J. Geophys. Res.* **80,** 4881–4888.

Jennings, P. C. (1979). The local magnitude of the Santa Barbara earthquake, as determined from strong-motion instruments, *Earthquake Notes* **49,** 14.

Kanamori, H. and D. L. Anderson (1975). Theoretical basis for some empirical relations in seismology, *Bull. Seism. Soc. Am.* **65,** 1073–1095.

Kanamori, H. and G. S. Stewart (1978). Seismological aspects of the Guatemala earthquake of February 4, 1976, *J. Geophys. Res.* **83,** 3427–3434.

Langston, C. A. and D. V. Helmberger (1975). A procedure for modeling shallow dislocation sources, *Geophys. J.* **42,** 117–130.

Lay, T. and H. Kanamori (1980). Earthquake doublets in the Solomon Islands, *Phys. Earth Planet. Interiors* **21,** 283–304.

Lee, W. H. K., C. E. Johnson, T. L. Henyey, and R. F. Yerkes (1978). A preliminary study of the Santa Barbara, California earthquake of August 13, 1978 and its major aftershocks, *U.S. Geol. Surv. Circular 797.*

Mellman, G. R. (1978). A method for waveform inversion of body-wave seismograms, *Ph.D. Thesis*, California Institute of Technology, Pasadena, 116 pp.

Miller, R. K. and S. F. Felszeghy (1978). Engineering features of the Santa Barbara earthquake of August 13, 1978, *Earthquake Engineering Research Institute*, California.

Pechmann, J. C. (1980). Tectonic implications of small earthquakes in the Central Transverse Ranges, California (submitted for publication).

Savage, J. C., W. H. Prescott, M. Lisowski, and N. King (1978). Strain in southern California; measured north-south regional contraction, *Science* **202,** 883–885.

Sylvester, A. G., S. W. Smith, and C. H. Scholz (1970). Earthquake swarm in the Santa Barbara Channel, California, 1968, *Bull. Seism. Soc. Am.* **60,** 1047–1060.

Wallace, T. C., D. V. Helmberger, and G. R. Mellman (1981). A technique for the inversion of regional data in source parameter studies, *J. Geophys. Res.* **86,** 1679–1685.

Whitcomb, J. H. and L. K. Hutton (1978). On the magnitude of the August 13, 1978, Santa Barbara, California earthquake, *Trans. Am. Geophys. Union* **59,** 1130.

Wyss, M. and J. W. Brune (1967). The Alaska earthquake of March 28, 1964; a complex multiple rupture, *Bull. Seism. Soc. Am.* **57,** 1017–1023.

SEISMOLOGICAL LABORATORY (252-21)
CALIFORNIA INSTITUTE OF TECHNOLOGY
PASADENA, CALIFORNIA 91125
CONTRIBUTION NO. 3404

Manuscript received April 13, 1981